

# Obesity Prediction with EHR Data: A deep learning approach with interpretable elements\*

Mehak Gupta<sup>1,†</sup>, Thao-Ly T. Phan<sup>3,4</sup>, H. Timothy Bunnell<sup>1,2</sup>, Rahmatollah Beheshti<sup>1,5,†</sup>

<sup>1</sup> Computer and Information Sciences, University of Delaware, Newark, DE, USA

<sup>2</sup> Department of Biomedical Research, Nemours Alfred I. duPont Hospital for Children, Wilmington, DE, USA

<sup>3</sup> Department of Pediatrics, Nemours Alfred I. duPont Hospital for Children, Wilmington, DE, USA

<sup>4</sup> Department of Pediatrics, Thomas Jefferson University, Philadelphia, PA, USA

<sup>5</sup> Epidemiology Program, University of Delaware, Newark, DE, USA

† Email: mehakg@udel.edu (MG), rbi@udel.edu (RB)

## ABSTRACT

Childhood obesity is a major public health challenge. Obesity in early childhood and adolescence can lead to obesity and other health problems in adulthood. Early prediction and identification of the children at a high risk of developing childhood obesity may help in engaging earlier and more effective interventions to prevent and manage this and other related health conditions. Existing predictive tools designed for childhood obesity primarily rely on traditional regression-type methods without exploiting longitudinal patterns of children’s data (ignoring data temporality). In this paper, we present a machine learning model specifically designed for predicting future obesity patterns from generally available items on children’s medical history. To do this, we have used a large unaugmented EHR (Electronic Health Record) dataset from a major pediatric health system in the US. We adopt a general LSTM (long short-term memory) network architecture for our model for training over dynamic (sequential) and static (demographic) EHR data. We have additionally included a set embedding and attention layers to compute the feature ranking of each timestamp and attention scores of each hidden layer corresponding to each input timestamp. These feature ranking and attention scores added interpretability at both the features and the timestamp-level.

## CCS CONCEPTS

• Computing methodologies • Machine learning • Machine learning approaches • Neural networks

## KEYWORDS

• Childhood obesity • Electronic health records • Temporal data • Deep learning • Long short-term memory • Transfer learning

## 1 Introduction

Childhood obesity is a major public health problem across the globe as well as in the US. In 2019, the prevalence of obesity was 18.5% affecting almost 13.7 million US children and adolescents aged 18 or less [1]. Childhood obesity can continue into adulthood and is known to be a major risk factor for chronic diseases such as diabetes, cancer, and cardiovascular diseases [2]. Preventing childhood obesity has been actively pursued in pediatric programs. However, decades of rigorous research have shown that prevention and management of obesity is not easy [3]. This is partly due to our limited understating of obesity and the complex interactions among a myriad of various factors, including biological and environmental ones, that are known to contribute to obesity. Additionally, considering the limited resources available to the healthcare systems, identifying children at the highest risk of developing obesity is another obstacle facing prevention

programs. In such a complex domain, predictive models have been shown to be effective in informing decision-makers and providers in designing and delivering more effective interventions.

In this study, we created a set of predictive models of childhood obesity using a longitudinal dataset of children derived from the electronic health records (EHR) of a large pediatric healthcare system. EHR data consists of clinical data along with its related temporal information. EHR datasets are generally very sparse and complex due to a large amount of information captured and irregular sampling. EHR relate to the records of patients' visits, which consist of conditions diagnosed, drugs prescribed, procedures performed, and laboratory results recorded in any visit. The number of unique condition diagnosis, drugs, procedures, and lab results collected in EHR datasets is generally huge. This leads to a very large feature (input) space for a prediction model, despite each visit having only a very small subset of total unique conditions, drugs, procedures, and measurements recorded. Due to the sparse feature space associated with each visit, we removed features which are absent or not recorded in more than 98% of the population.

Our models consider the temporal changes in the children's health patterns. A large body of research has shown that childhood obesity patterns are sensitive to different patterns of weight gain such that more acute and rapid weight gain predicts a different severity of obesity than more chronic and gradual weight gain [4]. The major limitation of existing obesity models is twofold. First, available obesity models focus on single (or only a few) future point prediction [5]. For instance, several models have been developed for predicting obesity at the age of 5 [6]. These single-point prediction models cannot be generalized to predict the future BMI trajectories starting from various points in early childhood and adolescence. Obesity is prevalent in all age groups in childhood and adolescence. This makes the application of these models limited, as they cannot assist in predicting obesity status in other ages. Second, using aggregated patterns instead of longitudinal patterns for developing the models. For obesity, this is a major limitation, since rigorous research has shown that longitudinal patterns of obesity-related indexes (such as body-weight) have a very strong correlation with the future obesity patterns [4]. Aggregating EHR datasets (e.g., by calculating the average values) loses valuable knowledge from this type of time-series datasets.

To fill this important gap in the field, we present a Recurrent Neural Network (RNN) architecture with Long Short-term Memory (LSTM) cells, which learns the patient representation from the temporal data collected over various visits of the patient. Additionally, as one of the major drawbacks of deep learning models like RNNs is the lack of interpretability, we have used embedding weights on the input layer and softmax activations on LSTM layers to calculate the importance of the features and attention weights for each input timestamp. The importance score for the features and attention weights for timestamps were used for visualization. Apart from the time series data, EHR data also contains static data that does not change with every visit. This data consists of sex, race, ethnicity and zip code for each patient. We used a separate feed-forward network for the static data.

Our models can predict the body mass index (or BMI, defined as height in kg over height squared in meter) of various ages. Having the estimated BMI values, we specifically look at the problem of classifying children as obese (above 95th percentile), and non-obese at the ages between 3 and 20 years according to the growth charts for children and teens provided by US Center for Disease Control (CDC) [7]. Compared to existing obesity predictive models in this domain, our model uses a much larger dataset (44 million rows with 68029 unique patients) for training and considers a larger set of confounders for predicting outcomes. Our model is based only on the standard EHR data already available in many hospitals. Some work used questionnaires [8], and census data to predict obesity [6]. We did not use any other external data, and as the features that we use are commonly recorded in any standard EHR system, our models can be readily applicable to many healthcare systems. This also means that our models can be used with no additional cost in collecting any external data. While we focus on an obesity-related problem, our approach should be usable for studying similar problems using EHR data.

The main contributions of this paper include presenting a prediction model that uses LSTM cell layers on multivariate irregularly spaced time series data to predict outcomes at 3 different time points in the future and proposing a mechanism to add interpretability to this model. Our mechanism adds interpretability at both feature-level and timestamp-level for the predictive task, which provides insights into important clinical events at individual and population levels. In our experiments, we perform comparisons between machine learning techniques that ignore temporality and our-RNN based models that capture temporality in the data and show that our models can achieve significantly better results.

## 2 Related Work

Clinical predictive models are becoming more and more prevalent [9]. Until recently most of the clinical predictive models were primarily developed based on regression and logistic regression or other types of statistical analysis [5]. Traditional methods (including the machine learning ones) are not very effective in capturing the non-linear and temporal relationships in the complex EHR data. Recently, deep learning techniques have shown a lot of success in clinical predictive modeling [10].

Many of deep learning studies in this domain use RNNs, which refer to a special set of deep neural architectures used on sequential datasets. Unlike basic feedforward networks, RNNs can learn long-term dependencies in temporal data by sharing parameters through the deep computational graphs. However, remembering long-term dependencies using RNNs generally faces the vanishing gradient problem where gradient values becoming too small. Hochreiter et al. [11] introduced the LSTM gating mechanism where the gradient can flow for long durations. These gates learn to keep important information and throw irrelevant information from previous time steps. This way, they pass on the important information in the network for long durations. For additional details about RNN and LSTM architectures, we refer the reader to [11, 12].

Many clinical predictive models have been developed using RNNs to predict various health problems like heart failure [13-15], diabetes [16], high blood pressure [17], and hospital readmission [18]. However, and despite the urgent need, there is not a lot of work done in the field of obesity predictive modeling leveraging large scale datasets and advanced machine learning techniques. Most of the existing work relies on traditional machine learning methods. Example studies include using logistic regression, linear regression [19-22], and the random forest [6]. Our study uses deep learning techniques to capture the temporal nature of the data.

One of the major drawbacks of deep learning models is the lack of interpretability. The lack of interpretability reduces the value of prediction models, especially in the medical domain. If medical practitioners cannot understand how the outcome is predicted by a model, relying on the model's outcomes will not be practical [23]. Many attempts have been made recently to make sense of the outcome of these models. Bahdanau et al. [24] proposed the attention mechanism which is used in NLP for machine translation. This attention mechanism can improve the interpretability at time-level, i.e., it gives attention scores to timestamps. However, for multivariate time-series, we also need to consider feature importance at each timestamp. Zhang et al. [25] used a hierarchical attention mechanism by using a convolutional operation. Choi et al. [26] develop an interpretable model with two levels of attention weights learned from two reverse-time GRU models. Jin et al. [27] used two separate RNN networks to compute attention weights in EHR temporal data. In our work, we continue the use of attention mechanisms to improve the interpretability of the RNN based models for multivariate time-series to get importance score for timestamps and then get the importance score for each feature in the timestamps.

## 3 Data

### 3.1 Dataset description

The EHR data used in this work was extracted from the Nemours Children Health System, which is a large network of pediatric health in the US, primarily spanning the states of Delaware, Florida, Pennsylvania, and New Jersey. The dataset is a portion of the larger PEDSnet dataset, containing EHR data from over 10 major US Children's Health Systems [28]. Inclusion criteria for patients in our dataset included: (i) at least 5 years of medical history, (ii) no evidence of type 1 diabetes, (iii) no evidence of cancer, sickle cell disease, developmental delay, or other complex medical conditions. An equal number of normal weight and overweight or obese patients were selected by random sampling from the normal weight population. The dataset was anonymized. All of the dates were skewed randomly per patient by +/- 180 days. All the data access and processing steps were approved by the Nemours Institutional Review Board. The project was reviewed by the Nemours Institutional Review Board. Our final cohort consisted of 44,401,791 records from 68,029 distinct patients. Each record captures the timestamp for a visit start and end time and all the condition, procedure, drug, and measurement variables recorded for that visit. It also contains demographic data for each patient. The medical codes are standardized terminologies of SNOMED-CT, RxNorm, CPT, and LOINC [29] for both clinical and demographic facts. Some facts about the data are listed in Table 1.

**Table 1: Characteristics of the cohort used in this study**

Name	Value
Total number of patients	68,029
Total number of visits	44,401,791
Avg. number of visits per patient	51
Number of females	31,014 (45%)
Number of males	37,015 (54%)
Age of a patient	0-20, Mean = 5
Race and Ethnicity	
White or Caucasian	33244
Black or African American	25329
Non-Hispanic or Latino	58894
Others	17834

## 3.2 Data Representation and Preprocessing

The EHR data extracted for this study consisted of 20,300 condition diagnosis variables, 10,167 procedure variables, 6,163 drug variables, and 7,693 lab-results (measurement) variables. We preprocessed the original data to represent all the condition and procedure variables as binary variables (1 if present and 0 if not recorded for the visit). Few drug variables were present as continuous variables in original data where the values contain information about the amount of drug prescribed to a patient during a visit. However, many drug variables were present as binary variables so after preprocessing we represented it as binary variables. Measurement variables in the cohort were present as continuous variables. These continuous variables were normalized during preprocessing for model training.

EHR data consists of patient records as a sequence of visits with each visit containing various medical codes. We represented EHR data using incremental representation where we first represent medical codes using code-level representation, then we use a code-level representation of all medical codes for each visit record and represent visits using visit-level representation, and then we use visit-level representation for each visit of each patient and represent patients using patient-level representation. More details about these representations are provided in sections below.

### 3.2.1 Code-level Representation:

In code-level representation, medical codes consist of all the unique condition, drug, procedure and measurement variables in the complete data. We denote condition codes with the vector  $C: \{c_1, c_2, \dots, c_{|C|}\}$  with a size of  $|C|$ , drug codes with the vector  $D: \{d_1, d_2, \dots, d_{|D|}\}$  with a size of  $|D|$ , procedure codes with the vector  $P: \{p_1, p_2, \dots, p_{|P|}\}$  with a size of  $|P|$ , and measurement codes  $M: \{m_1, m_2, \dots, m_{|M|}\}$  with a size of  $|M|$ .

### 3.2.2 Visit-level Representation:

We denote visit at time  $t$  as  $V_t$ , which is the concatenation of condition, drug, procedure and measurement code vectors. The size of  $V_t$  is  $|V_t|=|C| + |D| + |P| + |M|$ . We represented condition, drug and procedure codes for visit  $V_t$  as binary vectors  $C_t \in \{0,1\}^{|C|}$ ,  $D_t \in \{0,1\}^{|D|}$ , and  $P_t \in \{0,1\}^{|P|}$  respectively where “1” represents the presence of the corresponding code for a visit  $V_t$ . All the measurement variables were represented by the corresponding continuous values  $M_t \in \mathbb{R}^{|M|}$  for visit  $V_t$ . Fig. 1 depicts the visit-level representation of our EHR data. EHR data for each patient is the sequence of visit-level vectors for that patient.

### 3.2.3 Patient-level Representation:

Patient-level representation is the sequence of visit vectors for a patient. We denote patients  $S: \{s_1, s_2, \dots, s_{|M|}\}$  as  $S$ , where the  $i$ -th patient  $s_i$  with  $T$  visits is represented as matrix  $s_i \in \mathbb{R}^{|T| * |V|}$

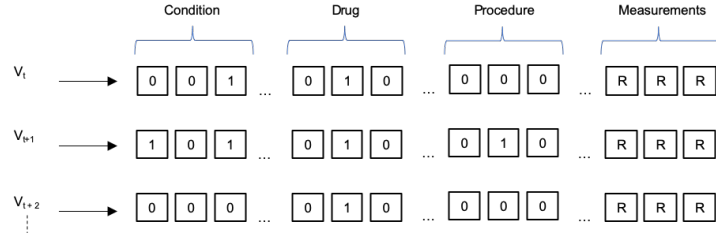


**Fig. 1 – Visit-level Representation of EHR data. Each visit  $V_t$  is represented as a vector of condition, drug, procedure and measurements variables. Collection of all visits for a patient forms a patient representation.**

In addition to the medical data which changes with each visit, the EHR data also consists of static demographic data which does not change with every visit. We represented demographic variables, i.e., sex, race, ethnicity, and zip code (indicating the approximate location of the patient) as categorical variables. Table 1 shows the distribution of race and ethnicity distributions in the data. Insurance information is also represented as a category variable.

The visit-level representation of complete EHR data consists of a large number of features including all unique conditions, drug, procedure, and measurement variables. Many of these features are not present in most of the population. We removed the features which do not have enough information and kept only the events that occurred in at least 2% of the population in the cohort to reduce the sparsity of the feature space. The total number of features in the final cohort was 1737.

The final data is extracted such that each patient has at least 5 years of data, and accordingly, sub-cohorts for every 5-year age range are created. We divided the complete cohort into 5 years of age ranges starting from the ages between 0 to 15 years, which resulted in 16 ranges (for the ages of 0 to 5, 1 to 6, ..., 15 to 20). Picking a longer range (more than 5 years of data) would have resulted in a small number of patients as there were fewer patients who have records of more than 5-year at one facility (due to various reasons like relocation and hospital change). For every 5-year data, we then used a fixed observation window of the initial 2-year and predicted obesity for 1, 2 and 3 years in the future. This way, we ended up with 48 sub-cohorts by creating 3 sub-cohorts for each of the 16 5-year time-periods. For each of the 48 models, we used only those patients with at least one visit in the observation and one visit in the prediction window. Fig. 2 depicts the way we created the sub-cohorts, the observation and the prediction window for these cohorts. The models are trained on data in the observation window to predict the future BMI value in the respective prediction window.

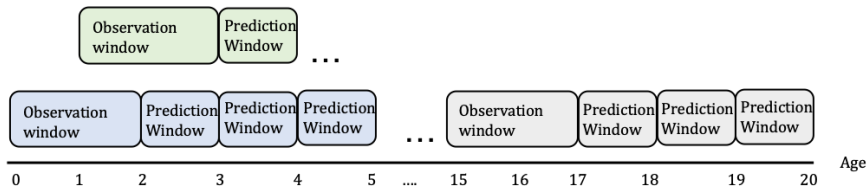


**Fig. 2 – Sub-cohort design plus observation and prediction window for each sub-cohort. For each observation window, there are 3 different prediction windows. As an example, note the observation window 0-2 years that is used for three prediction windows at age of 3 years, 4 years, 5 years.**

## 4 Method

Our proposed model is used to predict future BMI values, which are then used to classify patients as obese (above the 95th percentile) or non-obese (below the 95th percentile). The classification of BMI for different percentiles is done according to the BMI-for-age charts provided by the US Centers for Disease Control and Prevention (CDC) [7]. CDC tables label children based on age, gender and BMI for children from 24 months to 20 years of age. Children in the highest 5th percentile are labeled as obese. For infants aged from 0 to 2 years, classification is performed according to the Data Table of Infant Weight-for-age Charts, also provided by CDC [30].

## 4.1 Baseline Model

As briefly discussed in the Related Work Section, comparable predictive models of childhood obesity are not being used in clinical settings for screening or consulting (including at Nemours Health System where the data comes from). Therefore, to evaluate the performance of our proposed LSTM-based model, we created two baseline models that follow the traditional methods and aggregate the dataset while ignoring the temporality of the EHR data. We used linear regression and random forest regressors as the baseline models for comparison. To do this, we aggregated data over all the visits for each patient corresponding to any of the input sub-cohorts. All the visit records in the observation window are aggregated for each patient. Target labels will be the labels at the prediction age. Aggregation for binary medical codes of condition, drug, and procedure type is performed such that each medical code represents the frequency of its occurrence over the 2 years, and for continuous variables, we took the average over the 2 years. For the BMI and body weight, we took the maximum and latest BMI and bodyweight recorded in the observation window.

## 4.2 LSTM model

After obtaining all the sub-cohorts as explained in Section 3.2, we transformed the data so that it can be given as input to the LSTM model. Clinical visits obtained in Section 3.2 are represented by the medical codes associated with that visit. In general, (clinical) visits have irregular time intervals and each patient has a different number of visits. To transform these irregularly spaced and unequal number of clinical visits, we combined the visit data over a small fixed time window resulting in an equal number of time intervals. We combined visits over the 30-day time-periods for each observation window of the 2-year observation (training) windows, resulting in  $(2*365)/30 \sim 25$  equally spaced sequences for each patient. Fig. 3 shows how new sequences are obtained from unequal and irregularly spaced input time sequences. Any condition, drug and procedure variable observed at least once over 30-day time-period is denoted by 1 in new sequences. Continuous variables were averaged over the 30-day time-period. If there are no visits for a patient in any of the 30-day time-periods, the corresponding vector for that period contained all zeros. The zero vectors acted as padding to maintain equal sequence length for all patients. Such equally spaced time intervals between input time series are preferred representation for RNN models. In addition to conditions, procedures, drugs, and measurements the time intervals between each visit sequence (capture the time intervals between the non-empty sequences) were also added to the end of each visit's vectors. Adding time interval values has been shown to enrich the time-series input in similar studies [15].

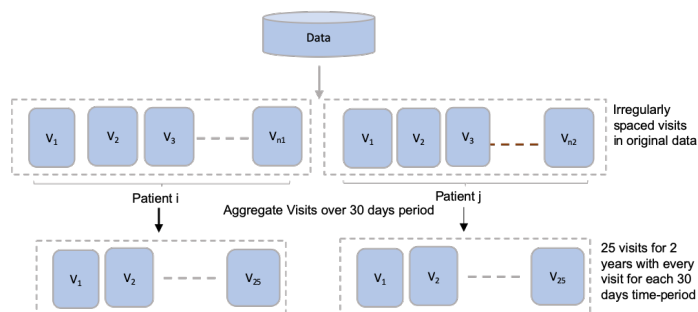


**Fig. 3 – Time sequences for the proposed LSTM model. Irregularly spaced visits for each patient (such as patient i and j) in each 2 year period is mapped to 25 equally distributed intervals.**

We used LSTM cells in the RNN for training our model over sequential visit-level (dynamic) data. The output of the LSTM layer was then concatenated with the set of demographics (static) data. This concatenated output is then passed through dense layers for predicting BMI value. The architecture of the complete model is shown in Fig. 4.

### 4.3 Interpretability

While deep learning models show superior performances compared to traditional machine learning models, they are difficult to interpret due to their so-called “black box” architecture [31]. This may reduce the practicality of deploying them in medical domains. To mitigate such concerns, we enhanced our basic LSTM model to add some level of interpretability. Refer to supplementary material Fig. S1 for basic LSTM model architecture. Because of the mixed nature of our datasets, we have considered two levels of interpretability as time-level and feature-level interpretability. Time-level interpretability refers to scoring visits, and feature-level refers to ranking features present in visits according to their importance in predicting the output. Fig. 4 shows the enhanced model architecture to achieve interpretability.

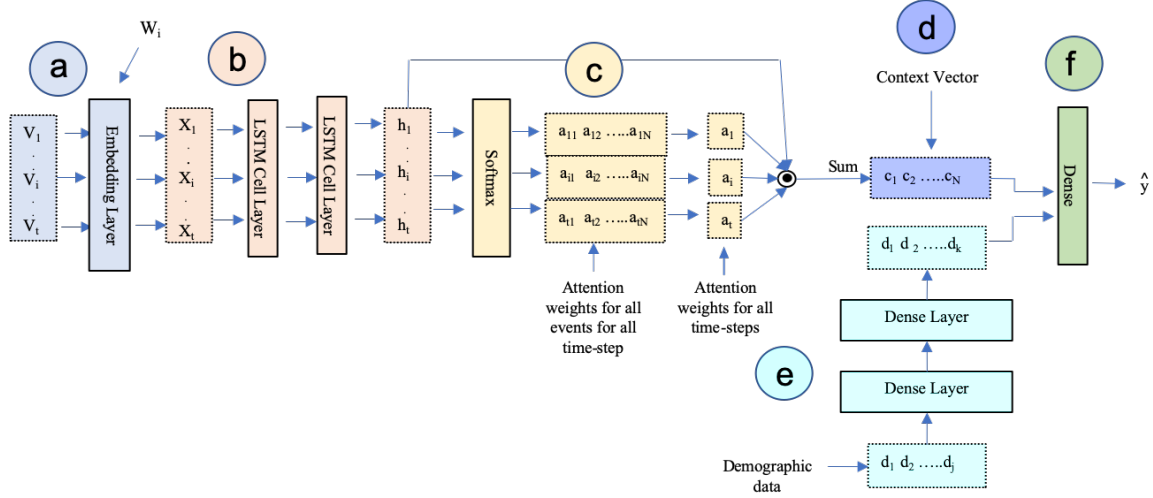


**Fig. 4 – Overview of proposed LSTM architecture with interpretability.** (a) visit-level input timestamp data ( $V_i$ ) for each patient. This data passes through embedding layer and embedding weights for this layer are denoted by  $W_i$  where  $i = \{1, 2, \dots, N\}$ , and  $N$  is the embedding layer dimension, (b) the output of the embedding layer passes through LSTM layers (2 LSTM layers) to provide hidden states  $h_1, h_2, \dots, h_t$ , (c) this hidden state passes through a softmax layer to generate attention scores for each  $h_t$  and all the codes in each timestamp as  $a_{t1}, a_{t2}, \dots, a_{tN}$ . We take average of values in  $\{a_{t1}, a_{t2}, \dots, a_{tN}\}$  vector to obtain scalar attention values  $a_t$  for  $h_t$ . (d) The scalar attention scores  $a_t$  are then used to take weighted sum of hidden state vectors  $h_t$  to obtain context vector  $c$  as  $\{c_1, c_2, \dots, c_N\}$ . (e) A separate feed-forward network is used for demographic data to obtain  $\{d_1, d_2, \dots, d_k\}$ , (f) concatenate vectors  $c$  and  $d$  and pass through the dense layer to obtain the output.

#### 4.3.1 Time-level interpretability

To enhance the interpretability at time level, we added a softmax layer on top of the LSTM layers to compute the “attention score” for each timestamp. In general, each LSTM unit generates a hidden output at each time step  $t$ , where  $t = \{1, 2, \dots, T\}$ . Hidden state  $h_t$  is computed by applying the non-linear transformation on input  $x_t$  to the LSTM unit at time  $t$  and hidden state of previous time step  $h_{t-1}$  (Eq. 1).

$$h_t \leftarrow \text{LSTM}(x_t, h_{t-1}) \quad (1)$$

where  $h_t$  is a vector of dimension  $N$  same as the dimension of the hidden layer of LSTM network. We calculated the attention score for each hidden by:

$$a_{t1}, a_{t2}, \dots, a_{ti}, a_{ti+1}, \dots, a_{tN} = \text{softmax}(h_t) \quad (2)$$

where  $h_t$  is of dimension  $|h_t| = N$  and  $N$  softmax scores are assigned to the  $h_t$  vector. To obtain scalar attention score value for each hidden state  $h_t$ , we took the average of all the values in the vector  $\{a_{t1}, a_{t2}, \dots, a_{ti}, a_{ti+1}, \dots, a_{tN}\}$  as shown in Eq. 2.

$$\mathbf{a}_t = \left( \sum_{i=1}^N \mathbf{a}_{ti} \right) \div N \quad (3)$$

The value  $a_i$  is calculated for each hidden state  $h_i$ . These scores are then used to compute the weighted sum of the hidden states (Eq. 4).

$$\mathbf{c} = \sum_{t=1}^T \mathbf{a}_t * \mathbf{h}_t \quad (4)$$

where  $\mathbf{c}$  is also a vector  $\{c_1, c_2, \dots, c_i, c_{i+1}, \dots, c_N\}$  of  $N$  dimension,  $|c| = N$  same as  $|h_i| = N$ . The vector  $\mathbf{c}$  obtained is then used to predict future BMI. The scores computed using the softmax layer are used to visualize the visits that are given most importance by the LSTM layer.

#### 4.3.2 Feature-level interpretability

To rank the input features in the multivariate time-series data, we added an embedding layer after the input layer and before the LSTM layer. We used weights from the embedding layer to compute the importance score for features in each timestamp. Softmax scores for the timestamp are multiplied (element-wise) with the embedding weight matrix for each input feature. Eq. 5 shows the  $s_i$  importance score calculation for  $i^{th}$  feature, where  $b_i = a_{i1}, a_{i2}, \dots, a_{ij}, a_{ij+1}, \dots, a_{iN}$  is the softmax score output after the LSTM layer and  $W_i$  is weight matrix for the  $i^{th}$  feature from the embedding layer.

$$s_i = W_i \odot b_i \quad (5)$$

## 4.4 Transfer Learning

Transfer learning is used to enhance model performance by learning from a larger dataset. While dividing our input data into the 48 sub-cohorts could improve its performance on learning specific age range patterns, this also meant reducing the input size of each of the models. This issue was especially more visible as the number of samples reduced gradually with increasing age ranges. Reduction in the number of samples in pediatric datasets is common due to the higher rate of visits in earlier years of children’s life. To improve the performance of the model, we used the complete dataset for all age ranges and created three initial models (instead of 48) for predicting obesity at 1 year, 2 years, and 3 years in the future respectively. After this, each of the three general models has been used as the basis for the 16 separate predictive models related to a similar prediction window.

## 4.5 Experiments

For training the LSTM models, we split data into 60:20:20 as training, validation and test data. Data split is performed such that the proportion of obese and non-obese samples is the same in the training and test data as in original data. Table 2 shows the number of obese and non-obese samples in each sub-cohort are shown in Table 2.

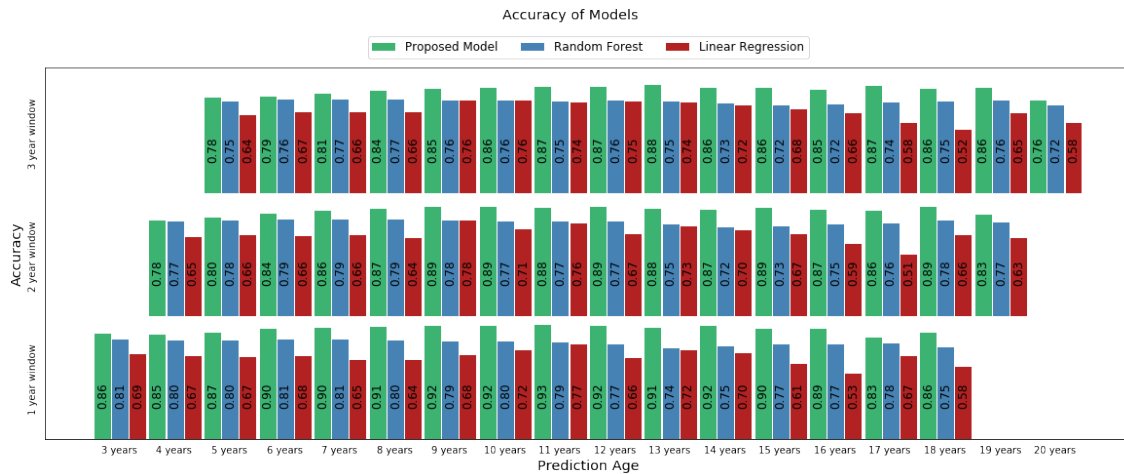
We used two LSTM layers for all models and an Adadelata optimizer [32] with an initial learning rate of 0.05. Both L1 and L2 regularizations were used on the first LSTM layer. Two fully connected layers were used for the feed-forward network for static (demographic) data that didn’t need to go through the LSTM layers. We trained different models on different sub-cohorts based on different observation window and prediction age as explained in section 3.2. All models are trained on data in the observation window to predict the future BMI value in the respective prediction window. The predicted BMI values were then used to classify each sample into obese and non-obese classes.

**Table 2 – Number of Obese and Non-obese Samples**

Observation Window (Age year)	Prediction Age (Age year)	# of Obese Samples	# of Non-Obese Samples
0-2	3, 4, 5	5556, 7492, 8192	27842, 25906, 25206
1-3	4, 5, 6	7382, 8081, 8307	25464, 24765, 24539
2-4	5, 6, 7	6697, 6878, 7014	19977, 19796, 19660
3-5	6, 7, 8	5697, 5788, 6216	16227, 16136, 15708
4-6	7, 8, 9	4840, 5194, 5679	13492, 13138, 12653
5-7	8, 9, 10	4428, 4813, 5117	11182, 10797, 10493
6-8	9, 10, 11	4085, 4368, 4574	9032, 8749, 8543
7-9	10, 11, 12	3773, 3941, 4047	7542, 7374, 7268
8-10	11, 12, 13	3273, 3354, 3387	6118, 6037, 6004
9-11	12, 13, 14	2671, 2729, 2692	4933, 4875, 4912
10-12	13, 14, 15	2116, 2078, 2078	3718, 3756, 3756
11-13	14, 15, 16	1507, 1502, 1530	2688, 2693, 2665
12-14	15, 16, 17	1052, 1059, 1087	1766, 1759, 1731
13-15	16, 17, 18	651, 665, 690	1044, 1030, 1005
14-16	17, 18, 19	250, 249, 260	358, 359, 348
15-17	18, 19, 20	55, 57, 55	87, 85, 87

## 5 Results

We compared the performance of the baseline models and our proposed LSTM model with interpretability trained on the larger dataset using transfer learning as explained in section 4.4. For the baseline models (linear regression and random forest regressor), we used 10-fold cross-validation and reported mean results over complete data. For the LSTM models, we did not use cross-validations (due to heavy computing cost) and only report results on test data. Fig. 5 shows the accuracy and AUC for all models separately based on the prediction window size. It compares the performance of 1) the Proposed LSTM model with interpretability trained using transfer learning, 2) Random Forest Regressor, 3) Linear Regression for each prediction window over different prediction windows separately. Refer to Table S1 in Supplemental Materials for an extended set of results of the proposed model. The additional baselines results discussed in Supplemental include result comparison for an additional variation of the proposed models which is the LSTM model without transfer learning. Fig. 6 demonstrates the effect of the size of the prediction window in predicting obesity at a certain prediction age. It compares the sensitivity, PPV, accuracy, and AUC of the proposed LSTM model with interpretability trained using transfer learning.



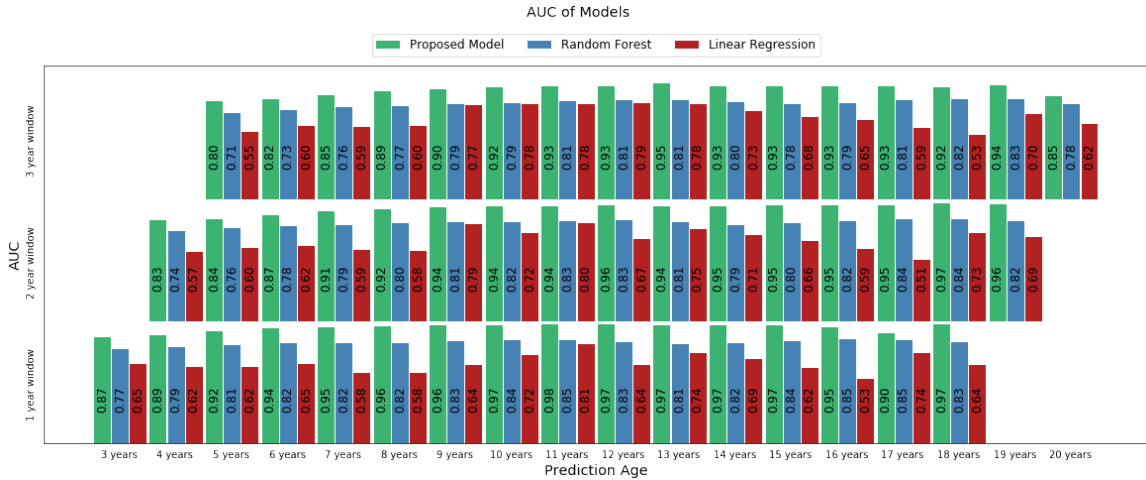


**Fig. 5 – Comparing accuracy and AUC results of 1) Proposed LSTM model with interpretability trained using transfer learning, 2) Random Forest Regressor, 3) Linear Regression. Separate results are shown for different prediction window – 1 year, 2 years and 3 years.**

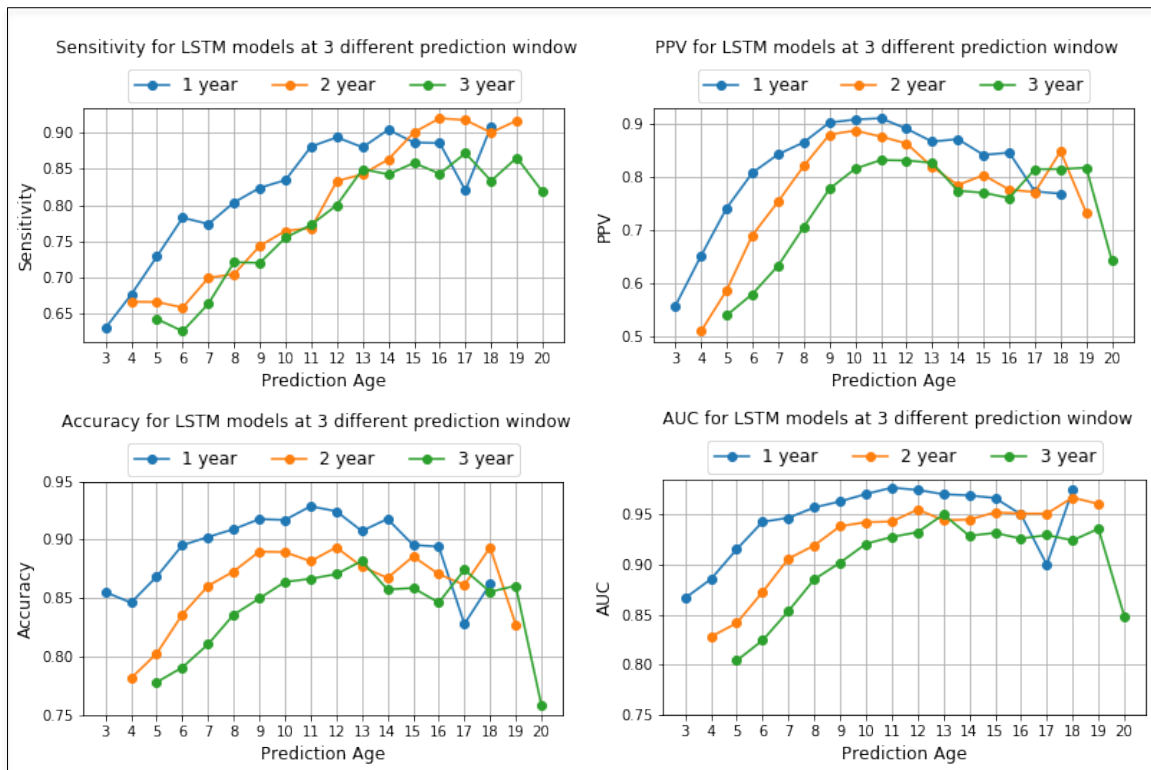


**Fig. 6 – Comparing the effect of the size of the prediction window in predicting obesity at a certain prediction age. Plots compare performance metrics. Sensitivity, PPV, accuracy, and AUC of LSTM with interpretability trained using transfer learning. Each plot compares the results obtained from different prediction windows for predicting obesity at a certain prediction age.**

Additionally, feature importance is computed at both the individual and population levels. Fig. 7 shows the ranking of the features in the top 3 important visits. Refer to Fig. S3 in Supplemental Materials for visualization of the attention weights given to input timestamps. This is the feature importance for a sample individual patient. The values in each cell in Fig. 7 is the measurement value for the corresponding feature.

We also ranked feature importance at the population level by averaging feature importance for the top 3 visits for all of the individual samples. Table 3 shows the top 20 most important features at the population level.

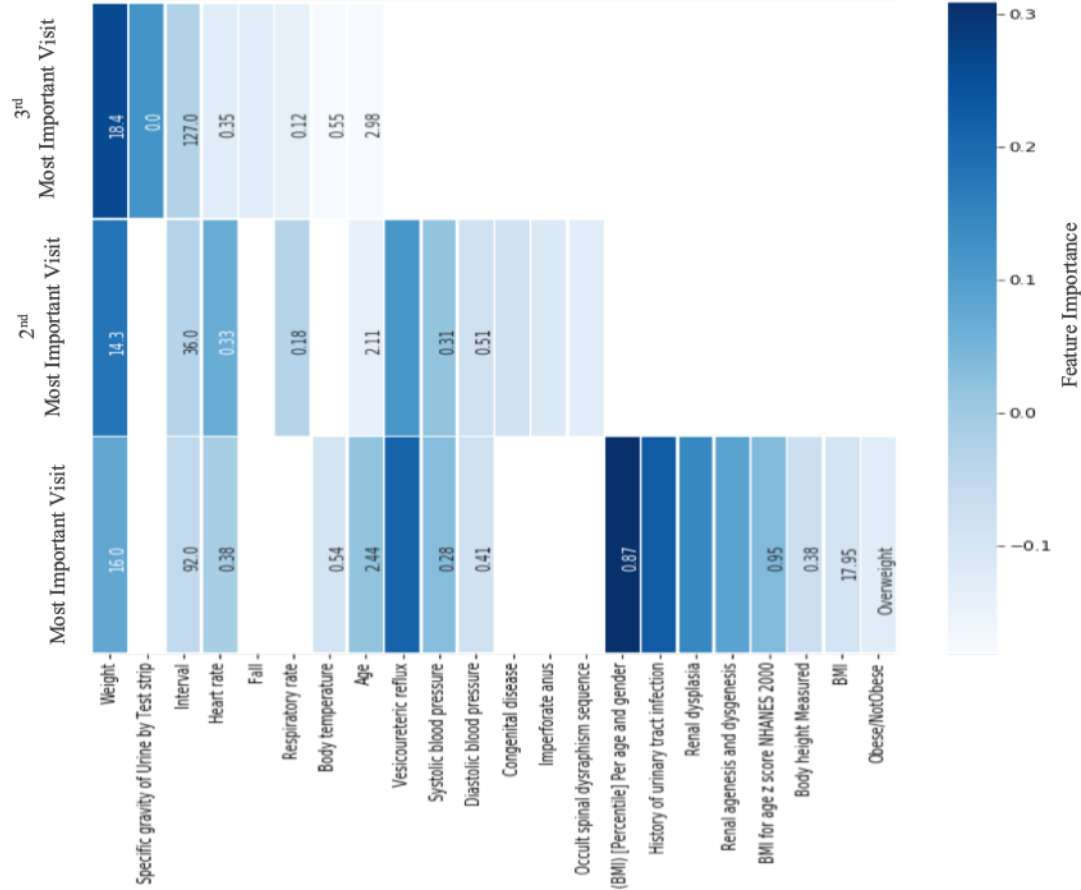


Fig. 7 – Ranking of the features for 3 most important visits (timestamps) for one patient (sample). Gradient bar on right shows the importance score for each feature present in the 3 timestamps, where darker shows more important. For measurement medical variables each cell shows the value associated with it. If the feature is condition variable than the corresponding cell is blank and only represents the existence of that condition.

Table 3. Feature rankings obtained by averaging the importance score of features obtained from all the samples in the test data.

Feature Ranking	Feature Description	Feature Ranking	Feature Description
1	BMI [Percentile] Per age and gender	11	Abnormal weight gain
2	Obese/Non-Obese Label	12	Anomaly of chromosome pair 21
3	Allergic urticaria	13	Erythrocytes (#/volume) in body fluid
4	Childhood obesity	14	Obesity
5	Morbid obesity	15	Hyperactive behavior
6	Suspected clinical finding	16	Tachycardia
7	Achondroplasia	17	Requires respiratory syncytial virus
8	MCH (Entitic mass) by Automated count	18	Vaccination
9	Cholesterol in LDL/Cholesterol in HDL	19	CO2 1712
10	Hearing loss	20	pH of Blood

## 6 Discussion

In this study, we have developed a new model for predicting childhood obesity patterns using EHR data. We employ an LSTM network and a separate feed-forward network to model dynamic (time-series) and static data in the EHR data. To transform the irregularly spaced and unequal number of clinical visits, we combined visits over the 30-day time window to obtain a regularly spaced equal number of clinical visits for each patient. The width of the fixed time window is related to the stability of clinical events for the prediction task. We experimented with different window sizes of 6 months, 3 months, 30 days and 15 days, and found out that a 30-day window size captures the variations in clinical trajectories of patients for predicting obesity.

As shown in Fig. 5, the performance of the LSTM was noticeably better than the two baseline models. i.e., linear regression and random forest. This shows that RNN architecture improves the prediction performance by taking into consideration the temporality of the data, a property that traditional methods do not have. The existing body of research shows that data temporality is important to capture weight gain trajectories and other medical histories over time [4]. Transfer learning helps further improves performance for the sub-cohorts with a low number of samples by learning from samples of other sub-cohorts. For instance, prediction at age of 20 using a 3-year window achieves accuracy and AUC of 0.45 and 0.55 respectively without using transfer learning technique, but when transfer learning is used, we achieved accuracy and AUC of 0.76 and 0.85 respectively. Refer to Fig. S2 for comparison of results obtained from training proposed model with and without transfer learning. Here transfer learning helps to improve the performance for this sub-cohort by learning from samples of other sub-cohorts.

As can be seen in Fig. 6, the closer the observation window is to the prediction time, the better the performance of the model. This means that the prediction results obtained using a 1-year prediction window are better than prediction results obtained using 2 years window which is better than prediction results obtained using 3 years prediction window. For both accuracy and AUC, all of the plots show a bell-shaped curve. In the beginning, the performance increases and then it starts to decrease after a certain prediction age. One reason for observing such a pattern could be decreasing in the number of samples and visits for that sub-cohort. There is a sharp decrease in performance for prediction at the age of 20 years. For prediction, at the age of 20 years, our model uses an observation window of 15 to 17 years of age, with a very small number of samples. This small number of samples in the observation window of 15 to 17 years has more impact on 3 years prediction window as compared to 1 and 2 years of prediction window.

The performance obtained from our proposed model is comparable to the performance of other studies for childhood obesity prediction[5, 6, 19, 33]. Our proposed deep learning model shows better performance compared to traditional machine learning model. In addition to superior predictive performance, we have also included interpretability capabilities to our proposed predictive model. We have ranked the features in each visit to provide insights into the prediction results. Specifically, we ranked the features for the three most important visits for a random sample to demonstrate the ability of our model to explain prediction for any sample. To do this, we picked the top three visits with the highest attention weights and then ranked the features for those visits by calculating their importance score using Eq. 5. In the case of the sample patient shown in Fig. 7, we can see that his/her previous weight and BMI are the most important features, which are naturally expected for predicting obesity. Among other highly ranked features, we can see that vesicoureteral reflux is given a very high importance score. This condition is a type of kidney disease which is highly correlated to obesity in children [34]. In addition to the feature ranking for the individual samples, we calculated the feature ranking over the complete dataset (with the samples that are predicted obese) to get population-level feature ranking. As shown in Table 3 most important population-level features in predicting childhood obesity as determined by our model. As expected, BMI and previous obesity levels recorded as obese/non-Obese Label, childhood obesity, morbid obesity, and obesity had the highest impact [35-37]. Other predictors of obesity with a lower prevalence that seemed to fit the existing body of knowledge were achondroplasia [38, 39] and the anomaly of the chromosome of chromosome 21 [40]. Hyperactive behavior has a known association with obesity though the direction of causality is undetermined. Obesity is known to be among the main risk factors of high LDL (bad) cholesterol and low HDL (good) cholesterol [41]. As obesity increases the risk for a variety of diseases, identifying suspected clinical findings among the top-ranked features is consistent with the current knowledge. MCH and Erythrocytes are shown to be related to chronic inflammation of obesity [42], and CO<sub>2</sub> and pH levels of blood may be related to obesity hypoventilation syndrome [43, 44]. Another suspected variable associated with obesity is listed as hearing loss, which is shown to be positively correlated with obesity [45]. Our results collectively show that feature

ranking obtained using the proposed LSTM model gives results that coincide with existing studies in the field of obesity research [46]. Similar to other predictive models, our models cannot show any causation relationship. However, identifying the top features that a model has been looking at may improve the explainability of our model.

Our work can be extended in several ways. In the future, we plan to add another attention layer after the initial dense layers for processing static (demographic) data. Moreover, in this work, we fixed the observation windows to only two years of data, in the future, we plan to employ the proposed model with a larger observation window size. Another future step would be expanding our transfer learning process by using data from other medical facilities.

## 7 Conclusion

In this study, we have developed a new deep neural network architecture for predicting future childhood obesity status in the next one, two, and three years. Specifically, we have used an LSTM-based for training our model using a longitudinal sample of patients' data obtained from a large US pediatric health system. An additional transfer learning process was used to improve the performance of the model developed for the sub-cohorts of the complete dataset. We showed that our LSTM-based model demonstrates a better performance as compared to traditional machine learning models that have been widely used in this important domain. For each sample, interpretability was achieved by ranking features in the top three most important visits during the two years of the training window. We have also calculated feature ranking for all samples in the data that were predicted obese in future. This gave us the list of features ranked according to their importance in predicting future obesity.

## References

- [1] C. f. D. C. a. Prevention. "Childhood obesity facts," <https://www.cdc.gov/obesity/data/childhood.html>.
- [2] W. H. Dietz, "Health Consequences of Obesity in Youth: Childhood Predictors of Adult Disease," *Pediatrics*, vol. 101, no. Supplement 2, pp. 518-525, 1998/03/01/, 1998.
- [3] S. Bleich, K. Vercammen, L. Zatz, J. Frelier, C. Ebbeling, and A. Peeters, "Interventions to prevent global childhood overweight and obesity: a systematic review," *The Lancet Diabetes & Endocrinology*, vol. 6, 10/01, 2017.
- [4] P. O. A. Monteiro, and C. G. Victora, "Rapid growth in infancy and childhood and obesity in later life—a systematic review," *Obesity Reviews: An Official Journal of the International Association for the Study of Obesity*, vol. 6, no. 2, pp. 143-154, 2005/05//, 2005.
- [5] N. Ziauddeen, P. J. Roderick, N. S. Macklon, and N. A. Alwan, "Predicting childhood overweight and obesity using maternal and early life risk factors: a systematic review," *Obesity Reviews*, vol. 19, no. 3, pp. 302-312, 2018.
- [6] R. Hammond, R. Athanasiadou, S. Curado, Y. Aphinyanaphongs, C. Abrams, M. J. Messito, R. Gross, M. Katzow, M. Jay, N. Razavian, and B. Elbel, "Predicting childhood obesity using electronic health records and publicly available data," *PloS One*, vol. 14, no. 4, pp. e0215571, 2019, 2019.
- [7] N. C. f. H. S. Centres for Disease Control and Prevention. "Data Table of BMI-for-age Charts," [https://www.cdc.gov/growthcharts/html\\_charts/bmiagerev.htm](https://www.cdc.gov/growthcharts/html_charts/bmiagerev.htm).
- [8] J. O. Robson, S. G. Verstraete, S. Shiboski, M. B. Heyman, and J. M. Wojcicki, "A risk score for childhood obesity in an urban Latino cohort," *The Journal of pediatrics*, vol. 172, pp. 29-34, 2016.
- [9] G. Bedogni, A. B. TsybakOv, and S. Berlin, "Clinical prediction models—a practical approach to development, validation and updating," *development*, vol. 18, no. 500, pp. 53-99, 2009.
- [10] B. Shickel, P. J. Tighe, A. Bihorac, and P. Rashidi, "Deep EHR: a survey of recent advances in deep learning techniques for electronic health record (EHR) analysis," *IEEE journal of biomedical and health informatics*, vol. 22, no. 5, pp. 1589-1604, 2017.
- [11] J. Schmidhuber, and S. Hochreiter, "Long short-term memory," *Neural Comput*, vol. 9, no. 8, pp. 1735-1780, 1997.
- [12] I. Goodfellow, Y. Bengio, and A. Courville, "Deep learning. vol. 1," MIT press Cambridge, 2016.

- [13] E. Choi, M. T. Bahadori, A. Schuetz, W. F. Stewart, and J. Sun, "Doctor ai: Predicting clinical events via recurrent neural networks." pp. 301-318.
- [14] E. Choi, A. Schuetz, W. F. Stewart, and J. Sun, "Medical concept representation learning from electronic health records and its application on heart failure prediction," *arXiv preprint arXiv:1602.03686*, 2016.
- [15] E. Choi, A. Schuetz, W. F. Stewart, and J. Sun, "Using recurrent neural network models for early detection of heart failure onset," *Journal of the American Medical Informatics Association*, vol. 24, no. 2, pp. 361-370, 2016, 2016.
- [16] T. Pham, T. Tran, D. Phung, and S. Venkatesh, "Deepcare: A deep dynamic memory model for predictive medicine." pp. 30-41.
- [17] Z. Liang, G. Zhang, J. X. Huang, and Q. V. Hu, "Deep learning for healthcare decision making with EMRs." pp. 556-559.
- [18] N. Wickramasinghe, "Deepr: a convolutional net for medical records," 2017, 2017.
- [19] A. Morandi, D. Meyre, S. Lobben, K. Kleinman, M. Kaakinen, S. L. Rifas-Shiman, V. Vatin, S. Gaget, A. Pouta, and A.-L. Hartikainen, "Estimation of newborn risk for child or adolescent obesity: lessons from longitudinal birth cohorts," *PloS one*, vol. 7, no. 11, pp. e49919, 2012, 2012.
- [20] M. Steur, H. A. Smit, C. M. A. Schipper, S. Scholtens, M. Kerkhof, J. C. De Jongste, A. Haveman-Nies, B. Brunekreef, and A. H. Wijga, "Predicting the risk of newborn children to become overweight later in childhood: the PIAMA birth cohort study," *International Journal of Pediatric Obesity*, vol. 6, no. sup3, pp. e170-178, 2011, 2011.
- [21] Y. Manios, M. Biribilis, G. Moschonis, G. Biribilis, V. Mougios, C. Lionis, and G. P. Chrousos, "Childhood Obesity Risk Evaluation based on perinatal factors and family sociodemographic characteristics: CORE index," *European journal of pediatrics*, vol. 172, no. 4, pp. 551-555, 2013, 2013.
- [22] C. Druet, N. Stettler, S. Sharp, R. K. Simmons, C. Cooper, G. Davey Smith, U. Ekelund, C. Lévy-Marchal, M. R. Jarvelin, and D. Kuh, "Prediction of childhood obesity by infancy weight gain: an individual-level meta-analysis," *Paediatric and perinatal epidemiology*, vol. 26, no. 1, pp. 19-26, 2012, 2012.
- [23] M. Peleg, S. Tu, J. Bury, P. Ciccarese, J. Fox, R. A. Greenes, R. Hall, P. D. Johnson, N. Jones, A. Kumar, S. Miksch, S. Quaglini, A. Seyfang, E. H. Shortliffe, and M. Stefanelli, "Comparing Computer-interpretable Guideline Models: A Case-study Approach," *Journal of the American Medical Informatics Association : JAMIA*, vol. 10, no. 1, pp. 52-68, 2003, 2003.
- [24] D. Bahdanau, K. Cho, and Y. Bengio, "Neural machine translation by jointly learning to align and translate," *arXiv preprint arXiv:1409.0473*, 2014, 2014.
- [25] J. Zhang, K. Kowsari, J. H. Harrison, J. M. Lobo, and L. E. Barnes, "Patient2Vec: A Personalized Interpretable Deep Representation of the Longitudinal Electronic Health Record," *IEEE Access*, vol. 6, pp. 65333-65346, 2018, 2018.
- [26] E. Choi, M. T. Bahadori, J. Sun, J. Kulas, A. Schuetz, and W. Stewart, "Retain: An interpretable predictive model for healthcare using reverse time attention mechanism." pp. 3504-3512.
- [27] Z. Jin, J. Yang, S. Cui, D. Gotz, J. Sun, and N. Cao, "CarePre: An Intelligent Clinical Decision Assistance System," *arXiv:1811.02218 [cs]*, 2018/11/06/, 2018.
- [28] "PEDSnet: A pediatric Learning Health System," <http://pedsnet.org>; <https://pedsnet.org/>.
- [29] "PEDSnet Common Data Model," <http://pedsnet.org>; <https://pedsnet.org/data/common-data-model/>.
- [30] N. C. f. H. S. Centres for Disease Control and Prevention. "Data Table of Infant Weight-for-age Charts," [https://www.cdc.gov/growthcharts/html\\_charts/wtageinf.htm](https://www.cdc.gov/growthcharts/html_charts/wtageinf.htm).
- [31] J. Krause, A. Perer, and K. Ng, *Interacting with Predictions: Visual Inspection of Black-box Machine Learning Models*, 2016.
- [32] M. D. Zeiler, "ADADELTA: An Adaptive Learning Rate Method," *arXiv:1212.5701 [cs]*, 2012/12/22/, 2012.
- [33] S. F. Weng, S. A. Redsell, D. Nathan, J. A. Swift, M. Yang, and C. Glazebrook, "Estimating Overweight Risk in Childhood From Predictors During Infancy," *Pediatrics*, vol. 132, no. 2, pp. e414-e421, 2013/08/01/, 2013.
- [34] "Vesicoureteral Reflux (VUR) | NIDDK," <https://www.niddk.nih.gov/health-information/urologic-diseases/hydronephrosis-newborns/vesicoureteral-reflux>.
- [35] E. M. Taveras, S. L. Rifas-Shiman, B. Sherry, E. Oken, J. Haines, K. Kleinman, J. W. Rich-Edwards, and M. W. Gillman, "Crossing growth percentiles in infancy and risk of obesity in childhood," *Archives of Pediatrics & Adolescent Medicine*, vol. 165, no. 11, pp. 993-998, 2011/11//, 2011.

- [36] K. K. Ong, and R. J. F. Loos, "Rapid infancy weight gain and subsequent obesity: systematic reviews and hopeful suggestions," *Acta Paediatrica (Oslo, Norway: 1992)*, vol. 95, no. 8, pp. 904-908, 2006/08//, 2006.
- [37] N. Stettler, B. S. Zemel, S. Kumanyika, and V. A. Stallings, "Infant weight gain and childhood overweight status in a multicenter, cohort study," *Pediatrics*, vol. 109, no. 2, pp. 194-199, 2002/02//, 2002.
- [38] J. T. Hecht, O. J. Hood, R. J. Schwartz, J. C. Hennessey, B. A. Bernhardt, and W. A. Horton, "Obesity in achondroplasia," *American Journal of Medical Genetics*, vol. 31, no. 3, pp. 597-602, 1988/11//, 1988.
- [39] C. Saint-Laurent, L. Garde-Etayo, and E. Gouze, "Obesity in achondroplasia patients: from evidence to medical monitoring," *Orphanet Journal of Rare Diseases*, vol. 14, no. 1, pp. 253, 2019/11/14/, 2019.
- [40] T. Foerste, M. Sabin, S. Reid, and D. Reddihough, "Understanding the causes of obesity in children with trisomy 21: hyperphagia vs physical inactivity," *Journal of intellectual disability research: JIDR*, vol. 60, no. 9, pp. 856-864, 2016/09/, 2016.
- [41] J. Vekic, A. Zeljkovic, A. Stefanovic, Z. Jelic-Ivanovic, and V. Spasojevic-Kalimanovska, "Obesity and dyslipidemia," *Metabolism: Clinical and Experimental*, vol. 92, pp. 71-81, 2019//03/, 2019.
- [42] J. Vuong, Y. Qiu, M. La, G. Clarke, D. W. Swinkels, and G. Cembrowski, "Reference intervals of complete blood count constituents are highly correlated to waist circumference: should obese patients have their own "normal values?"," *American Journal of Hematology*, vol. 89, no. 7, pp. 671-677, 2014/07//, 2014.
- [43] J. F. Masa, J.-L. Pépin, J.-C. Borel, B. Mokhlesi, P. B. Murphy, and M. Á. Sánchez-Quiroga, "Obesity hypoventilation syndrome," *European Respiratory Review: An Official Journal of the European Respiratory Society*, vol. 28, no. 151, 2019/03/31/, 2019.
- [44] B. Mokhlesi, "Obesity hypoventilation syndrome: a state-of-the-art review," *Respiratory Care*, vol. 55, no. 10, pp. 1347-1362; discussion 1363-1365, 2010/10//, 2010.
- [45] A. K. Lalwani, K. Katz, Y.-H. Liu, S. Kim, and M. Weitzman, "Obesity is associated with sensorineural hearing loss in adolescents," *The Laryngoscope*, vol. 123, no. 12, pp. 3178-3184, 2013/12//, 2013.
- [46] K. Sahoo, B. Sahoo, A. K. Choudhury, N. Y. Sofi, R. Kumar, and A. S. Bhadoria, "Childhood obesity: causes and consequences," *Journal of Family Medicine and Primary Care*, vol. 4, no. 2, pp. 187, 2015/04/01/, 2015.